

The spiral pattern rotation speed of the Galaxy and the corotation radius with GAIA DR2

W. S. Dias,^{1*} H. Monteiro,¹, J. R. D. Lépine², and D. A. Barros³

¹UNIFEI, Instituto de Física e Química, Universidade Federal de Itajubá, Av. BPS 1303 Pinheirinho, 37500-903 Itajubá, MG, Brazil

²Universidade de São Paulo, Instituto de Astronomia, Geofísica e Ciências Atmosféricas, São Paulo - SP, Brazil

³Rua Sessenta e Três, 125, Rio Doce, Olinda, 53090-393 Pernambuco, Brazil

Accepted 2019 April 24. Received 2019 April 22; in original form 2019 March 20

ABSTRACT

In this work we revisit the issue of the rotation speed of the spiral arms and the location of the corotation radius of our Galaxy. This research was performed using homogeneous data set of young open clusters (age < 50 Myr) determined from Gaia DR2 data. The stellar astrometric membership were determined using proper motions and parallaxes, taking into account the full covariance matrix. The distance, age, reddening and metallicity of the clusters were determined by our non subjective multidimensional global optimization tool to fit theoretical isochrones to Gaia DR2 photometric data. The rotation speed of the arms is obtained from the relation between age and angular distance of the birthplace of the clusters to the present-day position of the arms. Using the clusters belonging to the Sagittarius-Carina, Local and Perseus arms, and adopting the Galactic parameters $R_0 = 8.3$ kpc and $V_0 = 240$ km s⁻¹, we determine a pattern speed of 28.2 ± 2.1 km s⁻¹ kpc⁻¹, with no difference between the arms. This implies that the corotation radius is $R_c = 8.51 \pm 0.64$ kpc, close to the solar Galactic orbit ($R_c/R_0 = 1.02 \pm 0.07$).

Key words: Galaxy: kinematics and dynamics – structure

1 INTRODUCTION

The Gaia mission recently released its second set of data (DR2) (Gaia Collaboration et al. 2018a) which provides precise astrometric and photometric data for more than one billion stars with magnitude G less than 21. Among other scientific outcomes, a great improvement is expected in the understanding of the structure and dynamics of spiral arms of the Milky Way, thanks to the new data on spiral arms tracers. Among these, a major role will be played by the open clusters, due to their precise distance and ages that can be determined from the color magnitude diagrams.

The Milky Way is a grand design galaxy, as revealed by its large scale spiral structure (Georgelin & Georgelin (1976), Levine et al. (2006), Hou et al. (2009), Hou & Han (2014), Reid et al. (2014)). According to the classical theory (see Shu (2016) for a review), the arms are located between the inner and outer Lindblad resonances. The radius of corotation (R_c), where the velocity of rotation of stars coincides with the rotation velocity of the spiral arms (Ω_p), is a fundamental parameter, which divides the Galactic disk in two regions. The interstellar matter penetrates the arms in opposite directions, and the arms change from leading to

trailing at that radius. In one of the branches of the classical theory, the arms are small perturbations in the gravitational potential of the disk, like gravitational potential grooves or valleys, produced by the crowding of stellar orbits in some regions of the disk. The orbits of the stars constituting the arms are closed ones, which repeat themselves after each turn (in the rotating frame of reference of the arms), and this guarantees a relatively long lifetime to the spiral structure (Pichardo et al. (2003), Junqueira et al. (2013)).

In spite of its merits, the classical model is being seriously challenged. Another line of thinking considers that spiral arms are transient, appearing and disappearing in periods of time of a few hundred million years (Sellwood 2010). In that view, R_c is not an important reference, as it changes frequently. Others consider multiple spiral structures with distinct rotation speed (Quillen & Minchev (2005) and Quillen et al. (2018)), which would mean that several R_c coexist. Even among the researchers who adhere to the classical view of the spiral structure, there has been no consensus concerning the location of the R_c . Mishurov & Zenina (1999) and Dias & Lépine (2005) located it very close to the Solar orbit radius. However, Drimmel & Spergel (2001) located it at 6.7 kpc, Acharova et al. (2012) at 7 kpc, and Monguió et al. (2015) places it farther away than the Perseus arm. Recently, Michtchenko et al. (2018) explained

* E-mail: wiltonsdias@yahoo.com.br

the moving groups observed in the solar neighborhood based on a model which places Rc close to the Sun.

The lack of a consensus on Rc shows the urgency of making use of the unprecedented volume and quality of Gaia DR2 data to establish firm observational constraints to it. The purpose of the present work is twofold. Firstly, we present a set of open clusters that has been analyzed using the Gaia DR2 catalogue. Secondly, we make use of this sample of open clusters to perform a new determination of Rc . We adopt a method similar to that of [Dias & Lépine \(2005\)](#), which consists in integrating the orbits of the clusters back to their birthplaces. The clusters are believed to born in spiral arms, so that each cluster reveals the position of a spiral arm at a past time equal to its age. By comparing the past position of the arm with the present-day position, the rotation angle of the spiral structure during that interval of time is obtained. This method is straightforward and has the advantage that it does not require any model nor any unknown parameter, except for the rotation curve of the Galaxy. As will be discussed, the rotation curve is sufficiently well known.

This paper is organized as follows: in the next Section we describe the sample of open clusters. Section 3 presents the method of membership determination. In Section 4 we comment on the method adopted for determining the distances and ages of the clusters. In Section 5 we discuss the galactic rotation curves and the orbits of the open clusters. In Section 6 we present the approaches proposed to estimate the rotation speed of the spiral pattern and we present the results. We summarize the main conclusions and comment on their consequences in Section 7.

2 THE SAMPLE OF YOUNG OPEN CLUSTERS

We used the version 3.5 of the DAML02 catalogue ([Dias et al. 2002](#)) to select 441 clusters with ages lower than 50 Myr. In addition we also analyzed 154 open clusters with no age determined in DAML02, 31 clusters recently discovered by [Castro-Ginard et al. \(2018\)](#) and 52 clusters discovered by [Cantat-Gaudin et al. \(2018\)](#), looking for young open clusters. As detailed in Section 4, we performed the isochrone fit to the stars with membership greater than 0.51 in order to select the clusters younger than 50 Myr to compose our sample.

For each cluster we searched for the stars in the Gaia DR2 catalogue, using the central coordinates and the radius taken from the DAML02 catalogue. Since the cluster's radius may be larger than that given in the catalogue (see [Gaia Collaboration et al. \(2017\)](#)) we opted to use a region in the sky about 2 arcmin bigger than the area covered by the cluster. However, for the clusters with an apparent diameter less than 5 arcmin we searched for stars in an area 4 times the cluster area. In this way, we include virtually all possible members of the studied clusters.

Before determining the membership, we filtered the data following the recipe published by [Gaia Collaboration et al. \(2018b\)](#). After many tests we decided not to use the data of magnitude G. In this way we obtain the same values in the final results of the isochrone fit, but with smaller errors. In addition, the code converges

much faster, as discussed in detail by [Monteiro and Dias \(2019\)](#).

The sample with a complete vector (x, y, z, vx, vy, vz) of initial conditions to orbit integration is composed by 80 open clusters younger than 50 Myr. This final sample is relatively small mainly because of our choice to use only open clusters with parameters ($\mu_\alpha \cos \delta$, μ_δ , radial velocity, distance, age) determined from the Gaia DR2 catalogue, and of the additional condition that the clusters had to be approved in a visual inspection of the isochrone fit, as commented in the next section.

3 MEAN ASTROMETRIC PARAMETERS AND MEMBERSHIP DETERMINATION

In a 3D plot of the Gaia DR2 astrometric data ($\mu_\alpha \cos \delta$, μ_δ , ϖ) of the stars in the region of an open cluster, the members of the cluster appear in a clump. From the statistical point of view, the closer to the center of the clump is a star the greater the probability that it is a member of the cluster. So the membership problem can be formulated in the data space as a maximum likelihood one, based on the assumption of normally distributed uncertainties in proper motion and parallax as:

$$f(\mathbf{X}) = \frac{\exp\left(-\frac{1}{2}(\mathbf{X} - \boldsymbol{\mu})^T \boldsymbol{\Sigma}^{-1}(\mathbf{X} - \boldsymbol{\mu})\right)}{\sqrt{(2\pi)^k |\boldsymbol{\Sigma}|}} \quad (1)$$

where \mathbf{X} is the column vector ($\mu_\alpha \cos \delta$, μ_δ , ϖ) composed of the proper motion components and the parallax, $|\boldsymbol{\Sigma}| \equiv \det \boldsymbol{\Sigma}$ is the determinant of the covariance matrix $\boldsymbol{\Sigma}$ and $\boldsymbol{\mu}$ the mean column vector. The covariance matrix incorporates all uncertainties and their correlations, which are all given in the Gaia DR2 catalogue.

Because of the large volume of data in Gaia DR2 and the large number of clusters to be analyzed, the resolution of the equations above can take a considerable amount of computational time due to the matrix operations involved. So, we opted to estimate the membership in two steps, as performed in [Dias et al. \(2018b\)](#) and [Monteiro and Dias \(2019\)](#). First we use the proper motion following the procedure described in [Dias et al. \(2018a\)](#) to select the stars with membership greater than 0.50 based on that model. Then we fit a 1D parallax space assuming Gaussian distributions for the field as well as for the cluster stars. With the distribution parameters estimated (mean proper motion and parallax) used as initial parameters we applied Eq. 1 and the full variance and covariance data from Gaia DR2 to obtain final membership probabilities.

The solution of Equation 1 provides the membership probabilities and the mean and standard deviation of the proper motions and parallaxes for each analyzed cluster.

Finally, we used the stars with membership probability greater than 0.50 and individual radial velocities given in Gaia DR2 to estimate the mean radial velocities of the clusters. In this study we opted to use the mean and standard deviation (1σ) to represent the radial velocity of the cluster. As we use only the clusters with parameters estimated using Gaia DR2 data to compose a homogeneous sample, this was a limiting criterion. In the final sample of 80 open clusters,

15 clusters have their radial velocity determined for the first time.

In Table A1 we present the mean proper motion, mean parallax and mean radial velocity with the respective errors represented by the one standard deviation of the open clusters provided by the Eq. 1. In the table are also given the number of cluster members, the equatorial coordinates (α , δ) and the radius of each cluster.

4 DISTANCES AND AGES FROM THE ISOCHRONE FIT

The next step in our procedure was to perform the isochrone fit by considering the astrometric membership of the stars in the cluster's field. The main objective was to determine the parameters: distance, age, color-excess and metallicity. The method to obtain distances and ages by isochrone fitting is described in previous papers of our group, applied to UBVRI data (Caetano et al. 2015) and (Monteiro et al. 2017) and more recently, applied to Gaia DR2 data (Dias et al. 2018b) and Monteiro and Dias (2019). We used exactly the same procedures in this work.

The parameters distance and age were obtained by fitting Padova theoretical isochrones (Bressan et al. 2012) to clusters, applying the cross-entropy continuous multi-extremal optimization method, which takes into account Gaia DR2 photometric data guided by the astrometric membership. Briefly, the main goal of the cross-entropy is to find a set of parameters for which the model provides the best description of the data as per maximum likelihood definition. This is performed by randomly generating N independent sets of model parameters and minimizing the objective function used to transmit the quality of the fit during the run process. To estimate the final errors on fundamental parameters, we used Monte-Carlo technique, re-sampling in each run with a replacement in the original data set, to perform a bootstrap procedure. The isochrones are also re-generated in each run from the adopted IMF. The final fundamental parameters and the errors were estimated by the mean and one standard deviation of five runs.

In this work we opted to be very restrictive considering only the isochrone fit results which satisfy a visual inspection. Although this is not an objective criterion, the double check allowed us to debug the sample to include only the very best final results in the sample used in spiral rotation speed analysis.

For a number of open clusters of the final sample, we determined values of distance and age which are in disagreement with published ones. A detailed discussion of each case is unnecessary, since Dias et al. (2018b) and the results obtained for the control sample from Moitinho (2001) show that the procedures and results obtained with Gaia DR2 data are reliable. In addition, the CMDs with our fitted isochrones were clearly better than those from the literature. A more detailed discussion will be presented in a forthcoming paper dedicated to the new open cluster catalogue based on Gaia DR2 data.

In summary, our analysis of the rotation velocity of the arms and R_c is based on new homogeneous results obtained exclusively with Gaia DR2 data and with our methods developed to estimate astrometric membership and mean pa-

rameters, as well as distances and ages from non-subjective isochrone fit.

The final fit results obtained for each cluster are presented in Table A2¹.

5 THE ORBITS OF THE OPEN CLUSTERS AND THE GALACTIC ROTATION CURVE

The gravitational potential of the Galaxy can be explained by a model composed of an axisymmetric disk, a bulge, and a halo, with parameters adjusted in order to fit the rotation curve (Barros et al. 2016). In practice, the potential that provides the force field in the Galactic midplane, can be derived directly from the rotation curve, avoiding any discussion on the details of the model.

Results based on recent important surveys show that the rotation curve of the Galaxy is flat in the galactocentric radius interval of interest for this work, between about 6.5 kpc and 10.5 kpc. Since the orbits of the open clusters studied here are confined within this range, the shape of the rotation curve outside this interval has no influence. As examples of recently measured curves, see the one derived from maser sources (Rastorguev et al. 2017), that derived from the SEGUE and RAVE surveys (Sysoliatina et al. 2018), and from GAIA DR2 (Crosta et al. 2018). The new results are not discrepant with the older ones, like the HI + CO rotation curve of Fich et al. (1989) and those determined from high mass star forming regions with measured parallax and proper motion by Reid et al. (2014). For simplicity we adopted a flat rotation curve which has been fitted to different tracers by Barros et al. (2016), for which we have an analytic expression. All the rotation curves have to be normalized to the adopted rotation velocity of the LSR (V_0) and to the solar radius (R_0), since better values of these parameters became available. We selected the most recent results from the literature; the value $R_0 = 8.3$ kpc and $V_0 = 240$ km s⁻¹ were taken from Gillessen et al. (2017) and Reid & Dame (2016), respectively.

There is, however, a small departure from flatness, in the form of a narrow dip at about 9.2 kpc, on which there is not yet a consensus. This feature can be seen in the curves published by several authors, eg. Fich et al. (1989), but has most often been ignored. It was tentatively explained by Sofue et al. (2009) and by Barros et al. (2016) as being due to a ring of matter in the galactic disk. It cannot be excluded that the mass excess beyond the solar radius to be due to the Local arm, in which case it would only correspond to a sector of a ring, not extending along the whole galactocentric circle. Anyway, the important fact is that the dip does exist; in the absence of certainty on its nature, we adopt the description of the dip given by Barros et al. (2016), and more recently by Michtchenko et al. (2017), now slightly modified because of the new R_0 adopted here. We used two rotation curves to determine Ω_p and the location of R_c . One curve is flat close to the Sun (equation 2), and the other is flat with a narrow dip (width 0.39 kpc, depth 12.5 km s⁻¹) centered at 9.2 kpc

¹ The results of the parameters of the clusters as well as all the detailed plots of the isochrone fits are given in electronic format available at <https://wilton.unifei.edu.br/gaia-dr2/0Cgaia.html>.

(equation 3). Figure 1 presents the two curves, described by equations 2 and 3.

$$V_{\text{rot}}(R) = 303 \exp\left[-\frac{R}{4.7} - \frac{0.036}{R}\right] + 232 \exp\left[-\frac{R}{1400} - \left(\frac{3.72}{R}\right)^2\right] \quad (2)$$

$$V_{\text{rot}}(R) = Eq.2 - 12.5 \exp\left[-\frac{1}{2}\left(\frac{R-9.2}{0.39}\right)^2\right] \quad (3)$$

The present-day positions of the open clusters in the Galactic midplane, using a Cartesian coordinate system defined as follows, are obtained from the Galactic longitudes (l) and latitudes (b), derived from the equatorial coordinates α and δ , and the heliocentric distances.

In all the figures of this paper we used the Galactic Center at (0,0) as reference and the x-axis pointing to the Galactic rotation direction. The rotation is clockwise or the vector angular velocity is perpendicular to the x-y plane pointing in the direction of the paper. The y-axis positive points towards the Galactic anti-center and the Sun is situated at (0,8.3) kpc position.

To compute the heliocentric U and V velocities and the respective errors of each open cluster, we use the equatorial coordinates, distances, proper motions, and radial line-of-sight velocities, following the formalism described by Johnson & Soderblom (1987), with U positive towards the Galactic anti-center and V positive towards the direction of Galactic rotation. In order to pass to the local standard of rest (LSR) reference frame, we add the components of the solar motion $U_{\odot} = (-11.10 \pm 0.75) \text{ km s}^{-1}$ and $V_{\odot} = (12.24 \pm 0.47) \text{ km s}^{-1}$ (Schönrich et al. 2010). The errors of U_{LSR}, V_{LSR} velocities were determined by the usual propagation formula.

With the U_{LSR} and V_{LSR} velocities and the azimuths θ , and adopting the LSR velocity $V_0 = 240 \text{ km s}^{-1}$ (Reid & Dame 2016), we calculate the Galactocentric radial V_R and tangential V_{θ} velocities. For each open cluster, a vector with components $(R, \theta, V_R, V_{\theta})$ is used as initial conditions for the integration of the orbit.

The birthplace positions and uncertainties of the open clusters were determined following Dinescu et al. (1999). We considered Gaussian distributions for the radial line-of-sight velocities, proper motions, and heliocentric distances. The standard deviations of the distributions were taken as being the measured errors of the observables. The birthplace positions were determined in a Monte Carlo scheme, by integrating the orbits 1000 times from the generated Gaussian distributions. The birthplaces of the clusters were taken as the mean of the distributions of the results of the integrations, with the uncertainties represented by the standard deviations. As in Dinescu et al. (1999), the solar Galactic radius, the solar motion, and the velocity of the LSR were kept fixed in the integrations.

The numerical integrations of the equations of motion were performed by means of a fifth-order Runge-Kutta integration procedure, with a typical time step of 0.1 Myr. The orbits of the open clusters were integrated backwards, for a time interval equal to the age of each object. This procedure

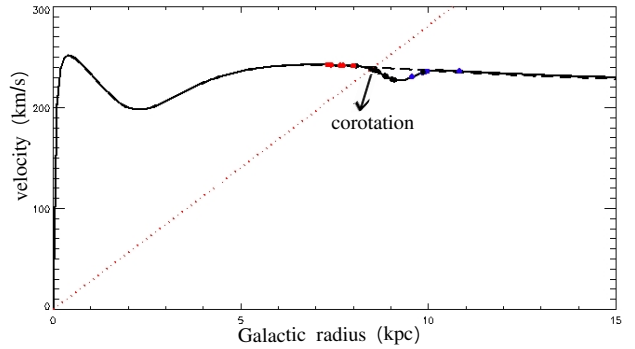


Figure 1. Rotation curves of the Galaxy which can be classified as plane and plane with a dip centered at 9.2 kpc. The functions of the curves are presented in the equations 2 to 3. The range of the Galactic distance of the sample of the open clusters and a respective arm is indicated by dots with color blue to Perseus, black to Local and red to Sagittarius-Carina. The dotted line indicates the spiral pattern rotation speed: $\Omega_p = 28.2 \pm 2.1 \text{ km s}^{-1} \text{ kpc}^{-1}$.

provided the initial positions X_0 and Y_0 , i.e. the birthplaces of the open clusters in the Galactic midplane.

Table A3 gives the present-day (X, Y) and the birthplace (X_0, Y_0) positions of the open clusters in the Galactic midplane. The errors in the present-day ($\sigma X, \sigma Y$) positions were obtained by the usual propagation formula while the errors in the birthplace positions were determined by Monte Carlo procedure as explained earlier.

6 METHOD, RESULTS AND DISCUSSIONS

The determination of the rotation speed of the spiral arms is based on the hypothesis that the birth of open clusters takes place in spiral arms. This follows from the ideas of Roberts (1969), Shu et al. (1972) and many others, according to whom the shock waves occurring in spiral arms are the triggering mechanism of star formation.

Therefore, every cluster carries with itself the evidence that a spiral arm was present at a given place (the birthplace) at a given epoch, specified by the age of the cluster. We find the birthplace of each cluster, integrating backward its orbit for time interval T equal to its age, starting from the present-day positions and space velocities, as discussed in the last section.

Basically, the birthplace of a cluster is supposed to represent a point of a spiral arm, a time T ago. So, if we rotate forward this point by an angle $\Omega_p T$ around the Galactic Center, we obtain a point situated on the present-day position of the arm. Therefore, for each birthplace of a cluster, we measure the galactocentric rotation angle that should be applied to make it coincide with the corresponding present-day spiral arm. Note that what is being rotated in this way back is a point of a spiral arm, and not the cluster. In this way, clusters with different ages produce independent measures of the rotation velocity, according to the equation 4 where the unknown parameter is Ω_p .

$$\theta_f = \theta_i + \Omega_p \times T \quad (4)$$

where, in polar coordinates, the azimuth θ_f is the present-day position angle of the arm, θ_i the birth-place position

angle of a cluster, Ω_p the rotation velocity of the arms, and T is the age of the cluster. We consider that the shape of the spiral arms is conserved, so that every point of the initial spiral arm has a corresponding point on the present-day arm obtained by a rotation angle $\Delta\theta = \theta_f - \theta_i$. The concept of present-day spiral arm is next discussed.

We adopted the present zero-age arms positions traced by masers sources since they are associated with massive O-B stars with lifetimes of the order of a Myr, which is small compared to the ages in our sample of clusters. We used the positions obtained from VLBI observations provided by Reid et al. (2014). Due to the lack of maser sources on the Sagittarius-Carina arm on its extension to $x \leq -1$ kpc, we completed the sample with HII regions data with photometric distances or distances from parallax given by Hou & Han (2014). As presented in Fig. 2 by the light-gray points and curves and also in the Figure 1 of Hou & Han (2014) the sample of masers and HII regions trace clearly the segment of the arms at present-day in the solar neighborhood.

We fitted polynomials with different degrees for each arm (degree 2 for Sagittarius-Carina, 1 for Local, 6 for Perseus) to the position of the masers, to obtain analytical description of the zero-age arms, in the regions of interest (the regions where we perform comparisons of the position of our sample of clusters with the arms). The reason for using polynomials instead of logarithmic spirals is that the arms are known to present local deviations with respect to the global logarithmic spirals, see eg. the case of the Sagittarius-Carina arm (Berdnikov & Chernin 1999; Xu et al. 2006). In the case of present work, the aim is not to obtain a satisfactory fit over a large region of the Galaxy, but the best fit possible over the small region of interest. The polynomial fit gives more liberty to the adjusted curve to run along the small deviations from spirals.

In Fig. 2 are presented the birthplace and the present-day Galactic position of the clusters of the sample as well the present-day position of the arms Sagittarius-Carina, Local and Perseus. It shows clearly that the young open clusters are tracers of the spiral structure, as has been known and used by many authors for different goals (e.g., Becker & Fenkart (1970); Russeil (2003)). The present-day locations of the clusters very closely follow the present-day locations of spiral arms based on masers and HII regions. This requires that the clusters have not moved out of the spiral arms over their lifetimes, which implies the cluster orbital motions must be close to that of the arm pattern. Indeed, looking at Fig. 2, one might even be able to see that the Sagittarius arm clusters slightly lead the arm, the Local arm clusters are pretty well centered, and the Perseus arm sources slightly tend to lag the arm. Such a pattern would be expected for corotation near the radius of the Local arm.

Note that only the correct value of Ω_p produces rotated positions coincident with the zero-age positions of the arms as can be seen in Fig. 3. The width of the arms used to test this coincidence is based on the work of Reid et al. (2014) which provides the intrinsic arm width using 103 regions of high-mass star formation measured with VLBI techniques. However, to accommodate the different values estimated for each arm as well as the uncertainties associated with the present-day and birth position of the open clusters we adopted a width of ± 0.3 kpc. If the rotated back position of a cluster did not fall within this distance from the zero-age

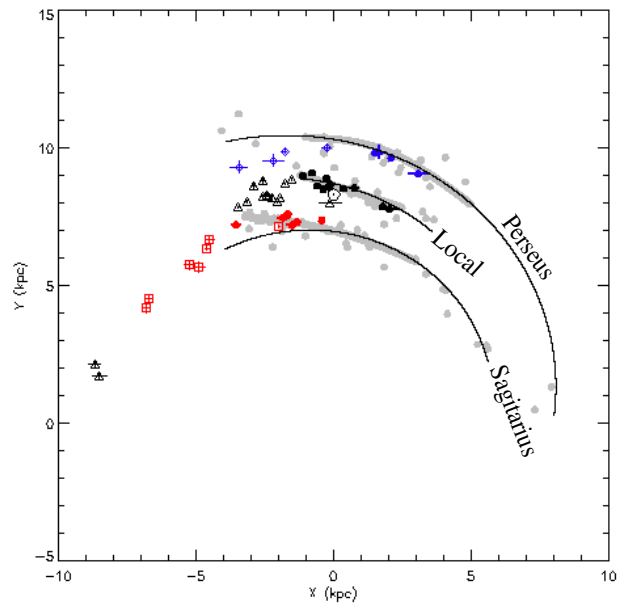


Figure 2. Location of the present-day positions (dots circles) and birthplace (open symbols) of the open clusters of the sample. In light-gray are the polynomials fit for present zero-age arms positions traced by masers and HII regions. The small range of each arm are restricted to the range of interest limited by the positions of the open clusters used in this study. The black line curves are log-periodic functions from Reid et al. (2014).

arm, this cluster was rejected. This occurrence depends on the adopted value of Ω_p . A fast converging process showed the value of Ω_p to be used. After calculating by the line fitting procedure described below, we entered the new Ω_p in the process above.

Considering the zero-age arms as reference for the measurements of the displacement of birthplaces of clusters we applied the following method to estimate Ω_p . We measure the angle $\Delta\theta$ that each cluster's birth position has to be rotated to coincide with the zero-age arm, as given in the equation 4. In Fig. 4 we present the plot with $\Delta\theta$ vs. the age of the cluster (ΔT).

The weighted linear least squares fit of $\Delta\theta$ vs. ΔT for each arm gives Ω_p , which is the slope of the fit. The best fit is given by minimizing the chi-square error statistic for a one parameter linear function, i. e., just the angular coefficient. The weights are given by the uncertainty associated with each measurement. Tab. 1 presents the results for Ω_p for each arm.

In Tab. 1 are also given the values of Ω_p obtained using the present-day arms described by spiral arms log-periodic functions as presented in Fig 2. To accommodate the uncertainty in the present-day spiral arms we opted to present the mean values determined considering polynomials and spiral arms log-periodic functions to describe the present-day arms local. The errors are obtained by combining quadratically the errors from each fit. In our opinion the polynomial and logarithmic spirals fits are in agreement in the region of interest of our work, which can be confirmed by the values of the Ω_p . The difference found for the Sagittarius arm is due to the difference between polynomials and spiral for $X < 0$,

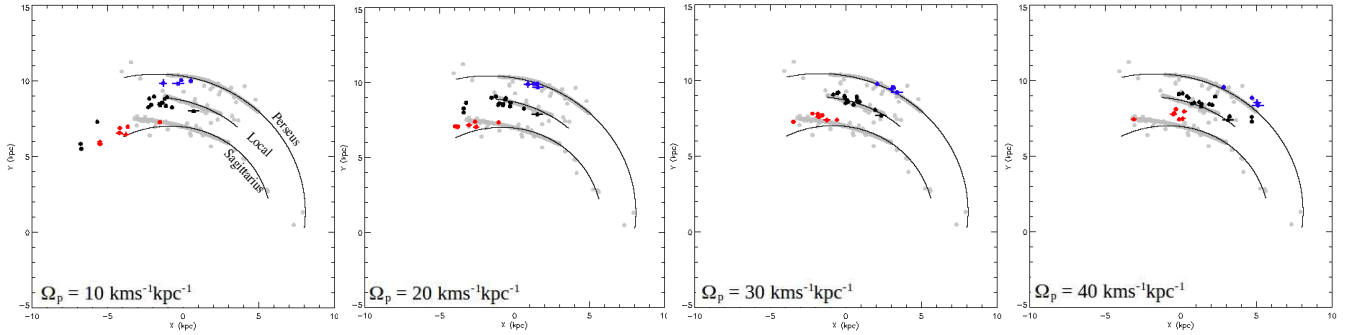


Figure 3. Present zero-age arms positions traced by masers and HII regions. The color dots are the returned positions of the arms reconstituted by $\Omega_p T$ from the birthplaces of the clusters, using different values of Ω_p . See Fig. 2 caption for other details. The final value of Ω_p is presented in the text.

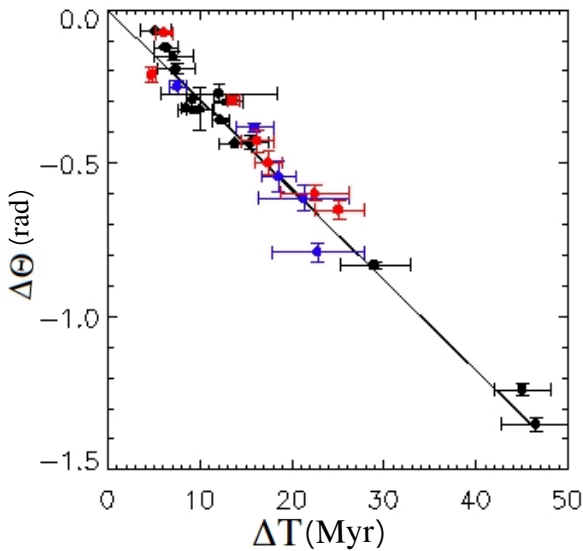


Figure 4. Weighted linear least squares fit of $\Delta\theta$ vs. ΔT . The slope gives the value of $\Omega_p = 28.2 \pm 2.1 \text{ km s}^{-1} \text{ kpc}^{-1}$.

due to the lack of maser data, where the open clusters are concentrated.

We also tested the dependence of the results with the age of the clusters of the sample performing the same procedures using sub-samples with different range in age. The Ω_p obtained from the complete sample were reproduced within the errors. This provides an observational evidence that arms do not have any angular acceleration at least in the last 50 Myr.

The derived corotation radius (R_c) obtained by $R_c = \frac{V_{rot}(R_c)}{\Omega_p}$ is $R_c/R_0 = 1.02 \pm 0.07$ from both rotation curves. In the Fig. 1 we present the Ω_p line over plotted to the Galactic rotation curves used in this study as commented in details in the last Section. The intersection of the curves indicates the R_c at about 8.5 kpc close the Galactic position of the orbit of the Sun. We neglect the fact that the Ω_p line crosses the dip at a rotation velocity smaller than 240 km s^{-1} , since the difference in velocity is very small.

It is interesting to point out we found an excellent agreement with the value of $R_c/R_0 = 1.06 \pm 0.08$ obtained in Dias & Lépine (2005), which were determined considering

Table 1. Ω_p (in $\text{km s}^{-1} \text{ kpc}^{-1}$) obtained with Galactic rotation curves from the equations 2 (plane curve) and 3 (curve with a dip centered at 9.2 kpc) adopting $R_0 = 8.3 \text{ kpc}$ and $V_0 = 240 \text{ km s}^{-1}$. The method used is the linear fit to $\frac{\Delta\theta}{\Delta T}$. In the first column are given the functions fitted used to the location of the zero-age arms: our polynomials (poly) and spiral arms log-periodic functions (spiral) from Reid et al. (2014). The value of all arms implies that the corotation radius is close to the solar Galactic orbit ($R_c/R_0 = 1.02 \pm 0.07$). See the text for details.

	arm	Eq. 2	Eq. 3
poly	all	28.1 ± 1.2	28.1 ± 1.3
	Pers	28.2 ± 1.7	28.4 ± 1.7
	Loc	28.6 ± 1.1	28.9 ± 1.1
	Car	27.3 ± 3.7	27.0 ± 3.6
spiral	all	28.4 ± 1.7	28.2 ± 1.6
	Pers	27.0 ± 1.7	26.1 ± 1.2
	Loc	27.7 ± 1.9	27.5 ± 1.8
	Car	20.9 ± 3.2	21.2 ± 3.2
mean	all	28.2 ± 2.1	28.2 ± 2.1
	Pers	27.6 ± 2.4	27.2 ± 2.1
	Loc	28.2 ± 2.5	28.2 ± 2.1
	Car	24.1 ± 4.9	24.1 ± 4.9

$\Omega_p = 25 \pm 1 \text{ km s}^{-1} \text{ kpc}^{-1}$, for $R_0 = 7 \text{ kpc}$ and $V_0 = 200 \text{ km s}^{-1}$.

Finally, the determined values of Ω_p show that there is no statistical distinction between the Ω_p of the different arms.

7 CONCLUSIONS

In this work, after exploring the Gaia DR2 data of several hundreds open clusters, we selected a sub-sample of young (age $< 50 \text{ Myr}$) objects situated within about 5 kpc from the Sun, and which presented the complete set of kinematic data and highest quality of the isochrone fit to the photometric data. We used the Gaia DR2 data to establish the stellar astrometric membership which were used to guide the isochrone fit performed by our global optimization tool to determine reliable and precise distance and age of the clusters. We used this homogeneous sub-sample completely based on the Gaia DR2 data to determine the spiral pattern rotation speed and the corotation radius of the Galaxy.

The method to determine Ω_p does not make use of any

model of the Galactic disc, except adopting an observed rotation curve taken from the literature, and assuming the widely accepted idea that the clusters are born in the spiral arms. A straightforward numerical integration of the cluster's orbits is performed to discover the position of the arms at a time T ago, equal to the age of the cluster.

The data of the spiral arm segments in the solar neighborhood, Sagittarius-Carina, Local, and Perseus, indicates that all the three arms were producing, during the last 50 Myr, a steady flow of clusters being born at a regular rate, at different distances from the present position of the spiral arm, as shown in Figure 4. There is no indication of any major burst-like periods of star-formation activity within the short time interval that we sampled.

In this study using a homogeneous data of open clusters, we determined Ω_p of the Galaxy to be 28.2 ± 2.1 km s⁻¹ kpc⁻¹, which implies that the corotation radius is located close to the solar Galactic orbit ($R_c/R_0 = 1.02 \pm 0.07$).

This result is in agreement with the classical interpretation and observations of the spiral structures, which place corotation about midway between the inner and outer Lindblad resonances (Canzian 1998), and is also consistent with previous results of our group (Dias & Lépine 2005).

The fact that corotation, the strongest resonance of the Galactic disk, is very close to the radius of the solar orbit, is essential for the understanding of the dynamics of the solar neighborhood, and is rich of consequences. This indicates that the Sun itself is probably trapped in the resonance and gives a hint on the dynamical origin of the Local arm (Lépine et al. 2017). It explains the main aspects of the moving groups (Michtchenko et al. 2018) and the step in the metallicity gradient observed by means of the open clusters (Lépine et al. 2011) probably associated with the high metallicity of trapped stars.

The presented results show that the Perseus, Local and Sagittarius-Carina arms rotate with the same angular velocity, within the errors of measurements. This means that there is no observational support for theories that consider arms with different velocities.

Finally, in our opinion the results should be more accurate with the Gaia final data. By improving our isochrone fit code, we may increase the sample of young open cluster with more precise distances and ages, and extend the age range.

ACKNOWLEDGEMENTS

We thank the referee Dr. Mark Reid for his valuable suggestions which improved the text. W.S.Dias acknowledges the São Paulo State Agency FAPESP (fellowship 2013/01115-6). H. Monteiro would like to thank FAPEMIG grants APQ-02030-10 and CEX-PPM-00235-12. This research was performed using the facilities of the Laboratório de Astrofísica Computacional da Universidade Federal de Itajubá (LAC-UNIFEI). This work has made use of data from the European Space Agency (ESA) mission Gaia (<http://www.cosmos.esa.int/gaia>), processed by the Gaia Data Processing and Analysis Consortium (DPAC), <http://www.cosmos.esa.int/web/gaia/dpac/consortium>). We employed catalogues from CDS/Simbad (Strasbourg)

and Digitized Sky Survey images from the Space Telescope Science Institute (US Government grant NAG W-2166).

REFERENCES

- Acharova I. A., Lépine J. R. D., Mishurov Y. N., 2012, *Astronomical and Astrophysical Transactions*, **27**, 359
- Barros D. A., Lépine J. R. D., Dias W. S., 2016, *A&A*, **593**, A108
- Becker W., Fenkart R. B., 1970, in Becker W., Kontopoulos G. I., eds, *IAU Symposium Vol. 38, The Spiral Structure of our Galaxy*. p. 205
- Berdnikov L. N., Chernin A. D., 1999, *Astronomy Letters*, **25**, 591
- Bressan A., Marigo P., Girardi L., Salasnich B., Dal Cero C., Rubele S., Nanni A., 2012, *MNRAS*, **427**, 127
- Caetano T. C., Dias W. S., Lépine J. R. D., Monteiro H. S., Moitinho A., Hickel G. R., Oliveira A. F., 2015, *New Astron.*, **38**, 31
- Cantat-Gaudin T., et al., 2018, preprint, ([arXiv:1805.08726](https://arxiv.org/abs/1805.08726))
- Canzian B., 1998, *ApJ*, **502**, 582
- Castro-Ginard A., Jordi C., Luri X., Julbe F., Morvan M., Balaguer-Núñez L., Cantat-Gaudin T., 2018, preprint, ([arXiv:1805.03045](https://arxiv.org/abs/1805.03045))
- Crosta M., Giammaria M., Lattanzi M. G., Poggio E., 2018, arXiv e-prints,
- Dias W. S., Lépine J. R. D., 2005, *ApJ*, **629**, 825
- Dias W. S., Alessi B. S., Moitinho A., Lépine J. R. D., 2002, *A&A*, **389**, 871
- Dias W. S., Monteiro H., Assafin M., 2018a, *MNRAS*, **478**, 5184
- Dias W. S., Monteiro H., Lépine J. R. D., Prates R., Gneiding C. D., Sacchi M., 2018b, *MNRAS*, **481**, 3887
- Dinescu D. I., Girard T. M., van Altena W. F., 1999, *AJ*, **117**, 1792
- Drimmel R., Spergel D. N., 2001, *ApJ*, **556**, 181
- Fich M., Blitz L., Stark A. A., 1989, *ApJ*, **342**, 272
- Gaia Collaboration et al., 2017, *A&A*, **601**, A19
- Gaia Collaboration Brown A. G. A., Vallenari A., Prusti T., de Bruijne J. H. J., Babusiaux C., Bailer-Jones C. A. L., 2018a, preprint, ([arXiv:1804.09365](https://arxiv.org/abs/1804.09365))
- Gaia Collaboration et al., 2018b, *A&A*, **616**, A10
- Georgelin Y. M., Georgelin Y. P., 1976, *A&A*, **49**, 57
- Gillessen S., et al., 2017, *ApJ*, **837**, 30
- Hou L. G., Han J. L., 2014, *A&A*, **569**, A125
- Hou L. G., Han J. L., Shi W. B., 2009, *A&A*, **499**, 473
- Johnson D. R. H., Soderblom D. R., 1987, *AJ*, **93**, 864
- Junqueira T. C., Lépine J. R. D., Braga C. A. S., Barros D. A., 2013, *A&A*, **550**, A91
- Lépine J. R. D., et al., 2011, *MNRAS*, **417**, 698
- Lépine J. R. D., Michtchenko T. A., Barros D. A., Vieira R. S. S., 2017, *ApJ*, **843**, 48
- Levine E. S., Blitz L., Heiles C., 2006, *Science*, **312**, 1773
- Michtchenko T. A., Vieira R. S. S., Barros D. A., Lépine J. R. D., 2017, *A&A*, **597**, A39
- Michtchenko T. A., Lépine J. R. D., Pérez-Villegas A., Vieira R. S. S., Barros D. A., 2018, *ApJ*, **863**, L37
- Mishurov Y. N., Zenina I. A., 1999, *A&A*, **341**, 81
- Moitinho A., 2001, *A&A*, **370**, 436
- Monguió M., Grosbøl P., Figueras F., 2015, *A&A*, **577**, A142
- Monteiro H., Dias W. S., Hickel G. R., Caetano T. C., 2017, *New Astron.*, **51**, 15
- Pichardo B., Martos M., Moreno E., Espresate J., 2003, *ApJ*, **582**, 230
- Quillen A. C., Minchev I., 2005, *AJ*, **130**, 576
- Quillen A. C., et al., 2018, *MNRAS*, **480**, 3132
- Rastorguev A. S., Utkin N. D., Zabolotskikh M. V., Dambis A. K., Bajkova A. T., Bobylev V. V., 2017, *Astrophysical Bulletin*, **72**, 122
- Reid M. J., Dame T. M., 2016, *ApJ*, **832**, 159

- Reid M. J., et al., 2014, *ApJ*, **783**, 130
Roberts W. W., 1969, *ApJ*, **158**, 123
Russeil D., 2003, *A&A*, **397**, 133
Schönrich R., Binney J., Dehnen W., 2010, *MNRAS*, **403**, 1829
Sellwood J. A., 2010, *MNRAS*, **409**, 145
Shu F. H., 2016, *ARA&A*, **54**, 667
Shu F. H., Milione V., Gebel W., Yuan C., Goldsmith D. W.,
Roberts W. W., 1972, *ApJ*, **173**, 557
Sofue Y., Honma M., Omodaka T., 2009, *PASJ*, **61**, 227
Sysoliatina K., et al., 2018, *A&A*, **614**, A63
Xu Y., Reid M. J., Zheng X. W., Menten K. M., 2006, *Science*,
311, 54

Table A1: Results of mean astrometric parameters obtained using the Gaia DR2 stellar proper motion and parallaxes. The meaning of the symbols are as follows: N_c is the number of cluster stars; R is the radius (in arcmin) used for each cluster to extract the Gaia DR2 data, centered on the coordinates of the cluster obtained from visual inspection. ϖ is the mean parallax of the cluster and $\sigma\varpi$ is the dispersion of the mean parallax. $\mu_\alpha \cos\delta$ and μ_δ are the proper motion components in mas yr^{-1} ; σ is the dispersion of cluster stars' proper motions; RV and σRV are the mean and 1σ dispersion radial velocity obtained for the cluster.

name	α	δ	N_c	R	ϖ	$\sigma\varpi$	$\mu_\alpha \cos\delta$	$\sigma\mu_\alpha \cos\delta$	μ_δ	$\sigma\mu_\delta$	RV	σRV
Alessi 20	00 10 22	+58 44 31	124	7.46	2.311	0.068	8.195	0.027	-2.341	0.028	-4.314	3.034
NGC 146	00 32 58	+63 20 03	197	3.32	0.311	0.026	-2.836	0.010	-0.454	0.007	17.840	17.630
King 16	00 43 45	+64 11 08	551	6.93	0.314	0.040	-2.654	0.040	-0.409	0.013	-42.961	0.919
Berkeley 4	00 45 01	+64 23 05	238	3.34	0.284	0.044	-2.421	0.013	-0.269	0.009	-53.130	1.190
NGC 366	01 06 26	+62 13 48	156	2.09	0.328	0.050	-2.060	0.011	-0.414	0.009	83.140	15.820
NGC 457	01 19 35	+58 17 12	1079	6.35	0.297	0.050	-1.578	0.006	-0.651	0.009	79.484	2.578
NGC 581	01 33 23	+60 39 00	237	3.18	0.370	0.032	-1.382	0.004	-0.504	0.010	-45.330	0.320
FSR 0551	01 39 45	+64 42 41	52	3.95	1.063	0.052	0.112	0.022	-1.422	0.021	-23.490	5.290
NGC 659	01 44 24	+60 40 24	272	3.17	0.272	0.050	-0.799	0.008	-0.276	0.010	77.810	17.610
Riddle 4	02 07 23	+60 15 25	117	2.72	0.337	0.050	-0.761	0.006	-0.523	0.007	-30.388	0.407
NGC 884	02 22 23	+57 07 33	1253	7.24	0.395	0.038	-0.607	0.007	-1.049	0.009	-43.525	0.284
IC 1805	02 32 50	+61 38 16	136	5.03	0.449	0.039	-0.702	0.015	-0.669	0.018	-40.930	3.990
ASCC 9	02 46 55	+57 43 48	525	8.33	0.391	0.034	0.156	0.012	-1.086	0.010	-72.118	2.037
Stock 23	03 16 11	+60 06 56	62	10.43	1.620	0.003	-4.286	0.005	-0.921	0.013	-16.298	6.274
Czernik 15	03 23 12	+52 15 00	74	2.58	0.309	0.050	0.396	0.007	-1.082	0.006	-84.820	1.800
Juchert 9	03 55 22	+58 23 28	39	1.34	0.186	0.087	-0.223	0.018	-0.033	0.023	-34.630	0.520
NGC 1502	04 07 49	+62 19 55	154	3.28	0.916	0.054	-0.571	0.016	-0.848	0.018	-14.760	6.480
ASCC 19	05 27 56	-01 59 13	188	25.37	2.768	0.089	1.152	0.019	-1.234	0.018	23.574	2.129
ASCC 21	05 28 43	+03 31 37	131	17.45	2.866	0.131	1.404	0.026	-0.632	0.022	16.034	3.808
Collinder 69	05 35 10	+09 48 47	669	37.42	2.462	0.124	1.194	0.021	-2.118	0.017	27.727	3.754
NGC 1980	05 35 24	-05 54 54	122	7.89	2.585	0.050	1.230	0.017	0.529	0.025	25.264	7.055
FSR 0850	05 45 15	+24 45 13	49	2.12	0.456	0.050	1.286	0.017	-2.518	0.010	19.370	1.350
Collinder 95	06 31 09	+09 53 38	144	6.77	1.458	0.117	-2.263	0.028	-5.159	0.026	8.726	0.595
NGC 2244	06 32 11	+04 54 50	623	9.02	0.617	0.127	-1.598	0.019	0.179	0.017	102.430	17.380
Collinder 107	06 36 49	+04 58 19	159	16.89	0.617	0.067	-1.325	0.015	0.659	0.013	131.600	7.420
NGC 2264	06 40 58	+09 53 42	667	13.27	1.355	0.050	-1.796	0.040	-3.651	0.011	19.006	4.567
vdBergh 92	07 03 54	-11 32 00	21	2.89	0.860	0.024	-4.469	0.013	1.461	0.010	25.600	11.310
Collinder 132	07 13 56	-30 45 29	99	61.20	1.501	0.087	-4.140	0.019	3.732	0.024	27.339	3.912
Collinder 135	07 17 27	-37 02 39	352	46.46	3.278	0.117	-9.975	0.027	6.157	0.025	16.719	2.325
NGC 2362	07 18 41	+24 57 14	165	2.74	0.742	0.074	-2.791	0.014	2.953	0.018	28.860	5.650
Ruprecht 18	07 24 39	-26 13 00	203	3.84	0.372	0.029	-0.495	0.006	1.159	0.007	31.403	0.373
Collinder 140	07 27 32	-31 57 58	150	22.07	2.594	0.105	-8.074	0.022	4.789	0.024	16.018	3.503
NGC 2414	07 33 12	-15 27 12	174	2.72	0.171	0.050	-1.393	0.006	1.460	0.014	194.970	3.020
NGC 2439	07 40 46	-31 41 38	551	3.15	0.232	0.047	-2.283	0.004	3.159	0.005	78.975	1.239
Haffner 13	07 40 50	-30 04 23	210	13.58	1.742	0.074	-6.184	0.018	5.879	0.015	33.488	7.284
NGC 2451B	07 44 31	-37 57 14	298	23.83	2.719	0.095	-9.671	0.034	4.702	0.025	22.791	2.739
Haffner 15	07 45 31	-32 50 46	175	1.80	0.238	0.051	-2.154	0.009	3.289	0.011	52.950	0.420
NGC 2453	07 47 35	-27 11 42	271	2.44	0.224	0.048	-2.346	0.012	3.430	0.020	64.721	0.333
Ruprecht 44	07 58 51	-28 35 00	468	4.87	0.172	0.034	-2.338	0.018	2.843	0.006	64.017	0.467
Pozzo 1	08 09 30	-47 20 06	390	22.00	2.853	0.102	-6.516	0.015	9.530	0.019	19.189	2.993
NGC 2547	08 10 09	-49 12 54	475	9.34	2.550	0.048	-8.611	0.051	4.257	0.041	12.139	2.064
IC 2395	08 42 30	-48 06 48	320	6.41	1.382	0.025	-4.385	0.017	3.199	0.009	23.197	4.154
Collinder 197	08 44 51	-41 14 00	154	6.98	1.029	0.050	-5.728	0.051	4.026	0.017	30.789	6.426
Trumpler 10	08 47 54	-42 27 00	151	11.51	2.263	0.050	-12.385	0.083	6.465	0.043	20.183	3.097
Alessi 43	08 50 17	-41 43 12	427	14.04	1.036	0.024	-5.472	0.032	3.931	0.029	67.870	15.330
IC 2581	10 27 29	-57 37 00	198	3.00	0.349	0.025	-7.254	0.020	3.614	0.016	-4.617	0.225
NGC 3293	10 35 51	-58 13 48	233	2.86	0.379	0.025	-7.671	0.032	3.350	0.019	-13.160	0.550
BH 99	10 38 13	-59 10 05	389	19.92	2.225	0.076	-14.494	0.016	0.919	0.017	11.617	6.317
Trumpler 15	10 44 43	-59 22 08	154	1.93	0.398	0.041	-6.209	0.019	2.016	0.012	16.590	0.290
Trumpler 18	11 11 28	-60 40 00	213	3.32	0.633	0.028	-7.168	0.011	0.583	0.018	-4.600	0.290
Ruprecht 94	11 30 37	-63 26 00	763	7.82	0.369	0.038	-6.366	0.013	0.886	0.020	1.633	1.097

NGC 3766	11 36 14	-61 36 30	837	4.37	0.460	0.035	-6.733	0.017	1.010	0.009	-16.489	0.269
Stock 14	11 43 48	-62 31 00	89	3.78	0.391	0.009	-6.364	0.018	0.847	0.021	-3.980	0.360
Collinder 359	12 02 24	+03 15 36	329	62.16	1.786	0.105	0.637	0.014	-8.668	0.015	-3.243	0.986
Basel 18	13 27 44	-62 18 46	117	3.10	0.526	0.030	-5.063	0.020	-2.081	0.039	12.240	0.390
Collinder 272	13 30 26	-61 19 00	466	4.31	0.420	0.033	-3.462	0.012	-1.861	0.019	-48.400	1.690
ASCC 79	15 18 55	-60 47 53	129	30.15	1.176	0.067	-2.914	0.036	-4.232	0.037	-4.619	7.764
NGC 6193	16 41 20	-48 45 48	130	4.65	0.823	0.046	1.401	0.019	-3.967	0.021	-14.539	3.860
Hogg 21	16 45 37	-47 44 00	234	2.63	0.347	0.035	-0.960	0.012	-2.174	0.008	-41.031	0.669
NGC 6216	16 49 24	-44 43 42	316	2.83	0.362	0.029	-1.245	0.017	-2.550	0.018	-34.870	0.400
BH 200	16 49 56	-44 11 00	108	2.62	0.409	0.039	-0.112	0.000	-1.026	0.006	-4.960	0.650
NGC 6231	16 54 10	-41 49 30	517	5.62	0.591	0.041	-0.569	0.006	-2.164	0.006	-28.470	15.750
ASCC 88	17 06 47	-35 36 00	1407	22.93	0.890	0.027	1.254	0.013	-2.256	0.018	-3.904	2.149
NGC 6322	17 18 30	-42 56 13	70	2.90	0.728	0.093	0.183	0.026	-2.272	0.023	-40.338	1.076
BH 231	17 31 56	-31 54 36	96	2.33	0.328	0.027	-0.851	0.011	-1.852	0.006	-11.340	0.320
Trumpler 28	17 36 55	-32 28 08	143	3.97	0.678	0.077	-0.851	0.021	-2.824	0.018	-15.810	1.310
Trumpler 33	18 24 42	-19 43 00	98	3.03	0.699	0.040	0.458	0.010	0.511	0.005	-4.640	0.380
NGC 6664	18 36 30	-08 11 38	237	4.49	0.468	0.059	-0.089	0.008	-2.561	0.008	-4.440	0.360
Roslund 2	19 45 24	+23 55 00	337	6.75	0.458	0.034	-1.789	0.018	-5.094	0.020	107.340	7.110
IC 4996	20 16 31	+37 39 19	143	2.16	0.479	0.029	-2.652	0.020	-5.272	0.013	-34.614	2.477
Berkeley 86	20 20 24	+38 42 00	143	3.31	0.572	0.041	-3.510	0.022	-5.497	0.027	-3.733	0.671
Teutsch 30	20 27 43	+36 04 32	23	1.77	0.534	0.018	-3.172	0.034	-5.682	0.024	94.080	14.030
NGC 7128	21 43 58	+53 42 54	180	1.64	0.261	0.061	-4.026	0.013	-4.111	0.011	-54.930	0.530
Alessi Teutsch 5	22 08 52	+61 06 11	158	15.61	1.111	0.062	-1.895	0.032	-3.207	0.018	-5.040	4.330
NGC 7235	22 12 25	+57 16 12	245	3.00	0.262	0.036	-3.777	0.012	-3.066	0.022	-57.120	0.190
Pismis Moreno 1	22 18 48	+63 16 00	45	3.38	1.057	0.029	-2.286	0.037	-2.250	0.015	1.650	9.840
Berkeley 96	22 29 49	+55 23 47	172	2.37	0.242	0.044	-3.511	0.013	-2.976	0.018	1.750	0.600
NGC 7380	22 47 21	+58 07 54	558	8.40	0.304	0.050	-2.624	0.015	-2.044	0.026	-51.118	2.610
NGC 7510	23 11 04	+60 34 44	324	2.36	0.286	0.048	-3.664	0.008	-2.193	0.008	63.740	3.440
Negueruela 1	23 47 24	+63 13 04	53	1.48	0.289	0.059	-2.988	0.031	-1.343	0.023	-5.020	2.940

Table A2: Results of fundamental parameters obtained from the isochrone fit. The distances are given in pc and ages in logt.

name	dist	σ_{dist}	age	σ_{age}	E(B-V)	$\sigma E(B-V)$	R _v	σR_v	Z	σZ
Alessi 20	436	12	6.975	0.087	0.26	0.05	3.27	0.36	0.010	0.001
NGC 146	2727	400	7.510	0.147	0.43	0.02	3.33	0.16	0.005	0.009
King 16	2494	101	7.203	0.056	0.67	0.04	3.02	0.17	0.002	0.001
Berkeley 4	2744	395	7.181	0.075	0.65	0.04	2.80	0.20	0.005	0.007
NGC 366	2667	254	7.302	0.087	0.94	0.07	2.91	0.20	0.003	0.004
NGC 457	2271	233	7.431	0.101	0.37	0.04	3.39	0.35	0.003	0.004
NGC 581	2061	258	7.336	0.069	0.34	0.04	3.38	0.36	0.003	0.005
FSR 0551	829	3	7.207	0.048	0.45	0.02	2.72	0.20	0.006	0.003
NGC 659	3018	260	7.436	0.077	0.55	0.02	3.13	0.17	0.009	0.005
Riddle 4	2270	371	7.328	0.099	0.74	0.06	3.39	0.26	0.003	0.006
NGC 884	1989	222	7.232	0.053	0.41	0.01	3.33	0.10	0.004	0.004
IC 1805	2158	211	6.878	0.055	0.73	0.08	2.56	0.35	0.019	0.004
ASCC 9	2047	105	7.268	0.035	0.81	0.06	2.56	0.17	0.002	0.001
Stock 23	726	32	7.641	0.084	0.33	0.02	2.45	0.24	0.030	0.009
Czernik 15	2605	295	7.491	0.071	0.89	0.07	2.30	0.22	0.003	0.006
Juchert 9	7632	1461	6.896	0.171	0.74	0.09	2.86	0.48	0.021	0.005
NGC 1502	1243	66	7.010	0.029	0.73	0.07	2.40	0.26	0.025	0.005
ASCC 19	354	12	7.141	0.053	0.07	0.02	2.70	0.24	0.021	0.004
ASCC 21	353	12	7.090	0.034	0.05	0.01	3.04	0.04	0.018	0.002
Collinder 69	401	9	6.965	0.036	0.10	0.01	3.02	0.03	0.014	0.002
NGC 1980	297	30	6.932	0.031	0.03	0.01	2.96	0.22	0.006	0.002
FSR 0850	1861	166	7.565	0.233	0.48	0.05	3.37	0.30	0.002	0.002
Collinder 95	630	51	6.715	0.143	0.19	0.12	2.16	0.26	0.053	0.008
NGC 2244	1304	29	6.904	0.120	0.44	0.01	2.63	0.09	0.005	0.003
Collinder 107	1328	26	7.146	0.026	0.41	0.03	2.64	0.20	0.004	0.001
NGC 2264	600	14	6.798	0.086	0.08	0.01	3.07	0.13	0.005	0.002
vdBergh 92	1085	124	6.852	0.132	0.30	0.04	2.23	0.20	0.034	0.003
Collinder 132	660	37	7.668	0.035	0.05	0.01	3.15	0.15	0.015	0.005
Collinder 135	310	8	7.575	0.029	0.07	0.01	2.87	0.17	0.018	0.002
NGC 2362	1285	123	6.872	0.120	0.17	0.03	2.25	0.26	0.005	0.004
Ruprecht 18	2317	181	7.676	0.155	0.57	0.04	3.15	0.23	0.004	0.002
Collinder 140	398	7	7.654	0.030	0.03	0.01	2.99	0.23	0.019	0.003
NGC 2414	4467	449	7.233	0.123	0.53	0.07	2.55	0.30	0.007	0.004
NGC 2439	2972	104	7.463	0.057	0.33	0.03	3.14	0.20	0.002	0.000
Haffner 13	529	14	7.560	0.043	0.07	0.00	2.04	0.07	0.013	0.002
NGC 2451B	370	9	7.557	0.028	0.09	0.01	2.90	0.18	0.018	0.003
Haffner 15	4686	144	7.141	0.011	0.81	0.04	3.11	0.15	0.023	0.001
NGC 2453	3556	96	7.321	0.107	0.38	0.02	3.48	0.17	0.002	0.000
Ruprecht 44	4339	308	7.358	0.095	0.44	0.03	3.37	0.20	0.008	0.002
Pozzo 1	341	3	7.073	0.030	0.08	0.02	2.24	0.10	0.011	0.001
NGC 2547	377	23	7.564	0.032	0.08	0.01	2.88	0.31	0.016	0.005
IC 2395	817	87	7.051	0.099	0.15	0.02	2.78	0.20	0.010	0.007
Collinder 197	594	25	7.111	0.039	0.47	0.05	3.24	0.29	0.003	0.001
Trumpler 10	442	10	7.627	0.016	0.05	0.01	2.71	0.15	0.019	0.002
Alessi 43	649	48	6.940	0.050	0.20	0.02	3.15	0.22	0.003	0.001
IC 2581	2272	220	7.151	0.031	0.35	0.02	3.03	0.16	0.007	0.006
NGC 3293	1769	120	7.137	0.039	0.27	0.03	2.78	0.23	0.002	0.002
BH 99	439	14	7.640	0.056	0.06	0.01	2.64	0.32	0.017	0.002
Trumpler 15	3691	195	6.681	0.028	0.47	0.05	2.83	0.31	0.042	0.004
Trumpler 18	1553	112	7.679	0.083	0.23	0.02	3.31	0.20	0.017	0.006
Ruprecht 94	1798	96	7.135	0.023	0.32	0.05	2.83	0.28	0.003	0.001
NGC 3766	1802	191	7.400	0.047	0.23	0.01	2.74	0.18	0.009	0.004
Stock 14	1989	256	7.211	0.045	0.28	0.02	2.42	0.08	0.008	0.005
Collinder 359	604	13	7.573	0.064	0.16	0.01	3.07	0.14	0.027	0.004
Basel 18	1869	281	7.242	0.038	0.29	0.01	2.96	0.13	0.016	0.010
Collinder 272	1652	195	7.353	0.072	0.51	0.06	2.42	0.31	0.003	0.005
ASCC 79	813	38	6.930	0.150	0.19	0.02	3.46	0.15	0.007	0.003
NGC 6193	1031	46	6.791	0.065	0.51	0.05	2.26	0.24	0.023	0.004

Hogg 21	2637	208	7.621	0.172	0.50	0.04	3.04	0.25	0.023	0.008
NGC 6216	2407	413	7.626	0.167	0.84	0.11	2.47	0.34	0.015	0.010
BH 200	1974	89	7.632	0.136	0.69	0.05	3.01	0.28	0.003	0.001
NGC 6231	989	72	7.095	0.035	0.50	0.03	2.29	0.18	0.003	0.001
ASCC 88	991	63	7.159	0.068	0.43	0.05	3.62	0.49	0.010	0.004
NGC 6322	1501	136	6.968	0.097	0.59	0.10	2.92	0.44	0.017	0.007
BH 231	2643	109	7.075	0.067	0.93	0.07	2.94	0.20	0.013	0.003
Trumpler 28	1380	78	7.503	0.035	0.57	0.02	2.94	0.08	0.017	0.006
Trumpler 33	1491	49	7.435	0.109	0.42	0.04	2.98	0.19	0.015	0.003
NGC 6664	1897	265	7.379	0.159	0.70	0.02	2.90	0.15	0.002	0.007
Roslund 2	1371	78	7.100	0.032	0.89	0.05	2.48	0.16	0.002	0.000
IC 4996	2124	399	6.999	0.063	0.55	0.05	2.64	0.23	0.012	0.009
Berkeley 86	1861	144	7.192	0.052	0.79	0.11	2.64	0.32	0.026	0.006
Teutsch 30	2492	207	7.506	0.139	0.95	0.04	3.02	0.17	0.022	0.003
NGC 7128	4824	908	7.145	0.217	0.92	0.12	2.57	0.33	0.019	0.011
Alessi Teutsch 5	804	9	7.118	0.051	0.40	0.04	2.38	0.30	0.006	0.002
NGC 7235	3737	145	7.309	0.061	0.82	0.06	2.55	0.19	0.010	0.003
Pismis Moreno 1	817	167	7.082	0.227	0.62	0.08	2.46	0.24	0.007	0.003
Berkeley 96	3196	404	7.268	0.044	0.52	0.05	2.73	0.22	0.006	0.005
NGC 7380	1810	497	7.352	0.039	0.52	0.03	2.85	0.07	0.002	0.010
NGC 7510	3497	99	7.100	0.040	0.86	0.02	2.78	0.07	0.015	0.002
Neguera 1	5691	370	6.822	0.035	0.92	0.08	3.00	0.26	0.036	0.004

Table A3: Present-day and birthplace positions of the open clusters and their respective errors. The x-axis pointing to the Galactic rotation direction and the y-axis positive points towards the Galactic anti-center. The Sun is situated at (0,8.3) kpc position. See the text for details

nome	X	σX	Y	σY	X_0	σX_0	Y_0	σY_0
Alessi 20	0.386	0.011	8.502	0.006	-1.929	0.030	8.177	0.010
NGC 146	2.341	0.343	9.699	0.205	-6.905	0.528	7.774	0.482
King 16	2.112	0.086	9.625	0.054	-1.749	0.083	9.871	0.067
Berkeley 4	2.320	0.334	9.764	0.211	-1.254	0.321	10.131	0.264
NGC 366	2.193	0.209	9.818	0.145	-4.683	0.354	8.293	0.221
NGC 457	1.817	0.186	9.651	0.139	-6.853	0.169	6.809	0.170
NGC 581	1.623	0.203	9.569	0.159	-3.351	0.212	9.250	0.160
FSR 0551	0.652	0.002	8.810	0.002	-3.130	0.076	8.341	0.039
NGC 659	2.332	0.201	10.214	0.165	-6.395	0.377	7.226	0.335
Riddle 4	1.680	0.275	9.825	0.249	-3.415	0.305	9.290	0.225
NGC 884	1.403	0.157	9.704	0.157	-2.495	0.180	9.605	0.139
IC 1805	1.533	0.150	9.819	0.148	-0.239	0.149	9.982	0.150
ASCC 9	1.376	0.071	9.815	0.078	-2.419	0.088	9.973	0.069
Stock 23	0.464	0.020	8.858	0.025	-8.764	0.126	4.606	0.229
Czernik 15	1.486	0.168	10.432	0.241	-4.548	0.254	10.290	0.209
Juchert 9	4.355	0.834	14.548	1.196	+2.355	0.661	14.794	1.296
NGC 1502	0.730	0.039	9.292	0.053	-1.820	0.066	9.186	0.063
ASCC 19	-0.141	0.005	8.603	0.010	-3.448	0.013	7.827	0.030
ASCC 21	-0.115	0.004	8.618	0.011	-3.131	0.018	8.058	0.046
Collinder 69	-0.103	0.002	8.679	0.008	-2.348	0.010	8.254	0.035
NGC 1980	-0.138	0.014	8.543	0.025	-2.220	0.022	8.198	0.060
FSR 0850	-0.115	0.010	10.156	0.166	-7.501	0.161	6.233	0.173
Collinder 95	-0.234	0.019	8.885	0.047	-1.500	0.011	8.832	0.051
NGC 2244	-0.579	0.013	9.468	0.026	-2.292	0.046	8.576	0.138
Collinder 107	-0.600	0.012	9.485	0.023	-3.347	0.048	7.277	0.104
NGC 2264	-0.231	0.005	8.853	0.013	-1.755	0.009	8.692	0.032
vdBergh 92	-0.761	0.087	9.072	0.088	-2.541	0.083	8.773	0.120
Collinder 132	-0.580	0.033	8.597	0.017	-8.375	0.217	1.557	0.102
Collinder 135	-0.284	0.007	8.409	0.003	-7.765	0.086	3.637	0.042
NGC 2362	-1.087	0.104	8.974	0.065	-2.891	0.092	8.614	0.091
Ruprecht 18	-1.997	0.156	9.459	0.091	-9.891	0.240	3.297	0.120
Collinder 140	-0.357	0.006	8.467	0.003	-8.551	0.185	2.017	0.081
NGC 2414	-3.490	0.351	11.084	0.280	-5.381	0.289	7.878	0.377
NGC 2439	-2.716	0.095	9.484	0.041	-7.508	0.099	5.178	0.078
Haffner 13	-0.479	0.013	8.523	0.006	-7.267	0.272	3.515	0.136
NGC 2451B	-0.350	0.009	8.412	0.003	-7.377	0.095	3.854	0.050
Haffner 15	-4.332	0.133	10.055	0.054	-7.439	0.100	8.355	0.102
NGC 2453	-3.176	0.086	9.899	0.043	-7.459	0.075	7.089	0.073
Ruprecht 44	-3.955	0.281	10.083	0.127	-8.477	0.251	6.963	0.227
Pozzo 1	-0.335	0.003	8.342	0.000	-3.117	0.029	7.724	0.020
NGC 2547	-0.371	0.023	8.335	0.002	-7.679	0.067	3.890	0.043
IC 2395	-0.814	0.087	8.349	0.005	-3.381	0.086	7.788	0.045
Collinder 197	-0.587	0.025	8.388	0.004	-3.446	0.069	7.642	0.052
Trumpler 10	-0.439	0.010	8.354	0.001	-7.817	0.137	1.979	0.042
Alessi 43	-0.643	0.048	8.383	0.006	-2.275	0.131	7.959	0.065
IC 2581	-2.199	0.213	7.727	0.055	-5.286	0.173	5.974	0.154
NGC 3293	-1.702	0.115	7.817	0.033	-4.900	0.100	6.317	0.079
BH 99	-0.421	0.013	8.175	0.004	-7.726	0.232	1.655	0.095
Trumpler 15	-3.522	0.186	7.196	0.058	-4.482	0.161	6.670	0.110
Trumpler 18	-1.450	0.105	7.743	0.040	-8.042	0.066	-0.518	0.157
Ruprecht 94	-1.641	0.088	7.568	0.039	-4.597	0.076	6.358	0.057
NGC 3766	-1.644	0.174	7.562	0.078	-6.791	0.123	4.183	0.181
Stock 14	-1.798	0.231	7.450	0.109	-5.226	0.188	5.756	0.173
Collinder 359	0.297	0.006	7.790	0.011	-6.944	0.040	3.700	0.029
Basel 18	-1.490	0.224	7.171	0.170	-4.873	0.213	5.663	0.197
Collinder 272	-1.308	0.154	7.291	0.119	-6.720	0.112	4.539	0.154

ASCC 79	-0.522	0.024	7.678	0.029	-2.586	0.063	7.358	0.048
NGC 6193	-0.406	0.018	7.353	0.042	-1.965	0.031	7.152	0.042
Hogg 21	-0.989	0.078	5.857	0.193	-5.866	0.225	-1.787	0.287
NGC 6216	-0.796	0.137	6.029	0.390	-5.585	0.472	-1.768	0.613
BH 200	-0.638	0.029	6.432	0.084	-7.079	0.091	0.154	0.114
NGC 6231	-0.283	0.021	7.353	0.069	-3.370	0.144	6.481	0.155
ASCC 88	-0.171	0.011	7.326	0.062	-3.675	0.050	6.592	0.062
NGC 6322	-0.381	0.034	6.850	0.131	-2.699	0.083	6.165	0.113
BH 231	-0.190	0.008	5.664	0.109	-2.819	0.068	4.914	0.096
Trumpler 28	-0.096	0.005	6.923	0.078	-6.102	0.106	2.692	0.095
Trumpler 33	0.320	0.011	6.846	0.048	-5.866	0.051	3.932	0.050
NGC 6664	0.770	0.108	6.566	0.242	-4.432	0.255	4.335	0.250
Roslund 2	1.190	0.068	7.619	0.039	-3.024	0.086	8.236	0.085
IC 4996	2.055	0.386	7.764	0.101	-0.105	0.403	8.012	0.019
Berkeley 86	1.810	0.140	7.870	0.033	-1.997	0.146	8.035	0.037
Teutsch 30	2.410	0.200	7.670	0.052	-7.882	0.355	7.827	0.354
NGC 7128	4.784	0.901	8.917	0.116	+1.460	0.706	10.534	0.584
Alessi Teutsch 5	0.776	0.009	8.501	0.002	-2.572	0.056	8.233	0.018
NGC 7235	3.645	0.141	9.121	0.032	-1.108	0.126	10.181	0.103
Pismis Moreno 1	0.779	0.159	8.533	0.048	-2.399	0.196	8.298	0.069
Berkeley 96	3.103	0.392	9.058	0.096	-2.177	0.380	9.497	0.227
NGC 7380	1.729	0.475	8.834	0.147	-3.183	0.439	8.400	0.265
NGC 7510	3.267	0.092	9.548	0.035	-1.156	0.094	9.783	0.054
Negueruela 1	5.123	0.333	10.776	0.161	+3.124	0.246	11.300	0.267

This paper has been typeset from a \TeX/L\AA\TeX file prepared by the author.

